

# Analysis of the metabolic deterioration of *ex vivo* skin from ischemic necrosis through the imaging of intracellular NAD(P)H by multiphoton tomography and fluorescence lifetime imaging microscopy

Washington Y. Sanchez  
Tarl W. Prow  
Washington H. Sanchez  
Jeffrey E. Grice

University of Queensland  
Princess Alexandra Hospital  
Therapeutics Research Centre  
199 Ipswich Road  
Brisbane, Queensland 4102  
Australia

Michael S. Roberts

University of Queensland  
Princess Alexandra Hospital  
Therapeutics Research Centre  
199 Ipswich Road  
Brisbane, Queensland 4102  
Australia  
and  
University of South Australia  
School of Pharmacy and Medical Science  
Adelaide, South Australia 5000  
Australia

**Abstract.** *Ex vivo* human skin has been used extensively for cosmetic and drug delivery studies, transplantable skin allografts, or skin flaps. However, it has a half-life of a few days due to ischemic necrosis. Traditional methods of assessing viability can be time-consuming and provide limited metabolic information. Using multiphoton tomography and fluorescence lifetime imaging (MPT-FLIM) we assess ischemic necrosis of *ex vivo* skin by NAD(P)H autofluorescence intensity and fluorescence lifetime. *Ex vivo* skin is stored in the presence and absence of nutrient media (Dulbecco Modified Eagle Medium) at  $-20$ ,  $4$ , and  $37$  °C and room temperature over a 7-day time course to establish different rates of metabolic deterioration. At higher temperatures we observe a decrease in NAD(P)H autofluorescence, higher image noise, and a significant increase in the average fluorescence lifetime ( $\tau_m$ ) from  $\sim 1000$  to  $2000$  ps. Additionally, significant distortions in NAD(P)H fluorescence lifetime histograms correspond to the reduction in autofluorescence. Skin kept at  $4$  °C, with or without media, showed the least change. Our findings suggest that MPT-FLIM enables useful noninvasive optical biopsies to monitor the metabolic state and deterioration of human skin for research and clinical purposes. © 2010 Society of Photo-Optical Instrumentation Engineers. [DOI: 10.1117/1.3466580]

Keywords: cells; multiphoton processes; image analysis; fluorescence.

Paper 09567RR received Dec. 21, 2009; revised manuscript received May 14, 2010; accepted for publication May 27, 2010; published online Aug. 4, 2010.

## 1 Introduction

Human *ex vivo* skin has been used as a model of *in vivo* epithelia for transdermal delivery,<sup>1</sup> for topical penetration studies,<sup>2,3</sup> and in cosmetic applications.<sup>4</sup> In addition, *ex vivo* skin is often used as a source of transplantable allografts<sup>4</sup> to treat burns and scalds, providing immediate barrier protection and pain relief while stimulating reepithelialization.<sup>5,6</sup> An issue in using *ex vivo* skin is maintaining viability and metabolic activity, as these are required to optimally simulate *in vivo* conditions for percutaneous penetration and to ensure the best clinical outcome for allograft recipients.<sup>4,7</sup> The most appropriate control for assessing the viability of *ex vivo* skin is *in vivo* skin, recognizing that *ex vivo* skin viability decreases over time as a consequence of ischemic necrosis. This is caused by the loss of blood supply after surgical excision, hypoxia, and the accumulation of toxic metabolites.<sup>8</sup>

Methods commonly used to assess the viability of *ex vivo* skin include the morphology of the tissue,<sup>9</sup> metabolic activity by MTT,<sup>10–12</sup> lactate dehydrogenase (LDH) activity assays,<sup>13</sup>

skin pH,<sup>14</sup> and oxygen consumption.<sup>11,15,16</sup> Several studies have used the MTT assay to measure the decreasing viability of *ex vivo* skin.<sup>7,8,11,17,18</sup> The MTT assay, which measures tetrazolium reduction by metabolic enzymes, is a technique widely used by researchers and skin banks for estimating the metabolic viability of *ex vivo* skin.<sup>2,18,19</sup> However, the measurement of metabolic viability by tetrazolium-based assays is limited, as it does not yield direct and real-time cellular information. This assay is also limited by the necessity to destroy the tissue, which restricts clinical applicability.

Several other methodologies have been used to assess skin viability including trypan blue dye exclusion, oxygen consumption, histopathological examination, and pH change.<sup>11,15,16</sup> Oxygen consumption and pH measurements have both been used to monitor skin metabolism noninvasively. Stratum corneum pH is considered to be critical for maintaining outer barrier function at pH 4.2 to 5.6. Therefore, alterations in skin surface pH indicate a potential disruption in that barrier. Messenger et al.<sup>15</sup> showed that both excised and frozen skin had a much higher pH ( $> \text{pH } 8$ ) and that over time the pH of the fresh skin decreased ( $< \text{pH } 7.5$ ), while the pH of the frozen skin did not change. Oxygen consumption is a

Address all correspondence to: Michael Roberts, Therapeutics Research Centre, University of Queensland Princess Alexandra Hospital, Brisbane, Queensland, Australia. Tel: 61-7-3240-5803; E-mail: m.roberts@uq.edu.au

hallmark of aerobic respiration and activity relates to the activity of mitochondria. Metabolic activity is especially critical for epidermal function. This important index of skin viability is closely related to NAD(P)H lifetime imaging, also tightly coupled to metabolic and mitochondrial activity.

Overall, both pH and oxygen consumption yield different but complementary information about skin viability to NAD(P)H imaging by multiphoton tomography and fluorescence lifetime imaging (MPT-FLIM). Oxygen consumption measurements have the advantage of low cost and ease of use, but the limitations include a lack of resolution in terms of which cells or layers of the skin are the most active or impaired. On the other hand, MPT-FLIM is a relatively expensive technique in terms of equipment, technical expertise, and data processing time required to obtain useful information, but has the advantage of subcellular resolution and multiple types of data output (i.e., microenvironment changes, semi-quantitative concentration, physical distribution of metabolic species, and morphological information).

Reduced nicotinamide adenine dinucleotide (NADH) and reduced nicotinamide adenine dinucleotide phosphate (NADPH) have also been used as metabolic indicators for the viability of cells and tissues.<sup>20–23</sup> Recently, fluorescence lifetime imaging microscopy (FLIM) analysis of intracellular NAD(P)H has been used to monitor metabolic activity in healthy and diseased tissue.<sup>24–27</sup> NAD(P)H refers to the summation of the molecules NADH and NADPH. The fluorescence lifetime ( $\tau$ ) of a molecule is the average time the molecule stays in the excited state.<sup>28</sup> FLIM can distinguish between compounds with similar fluorescence spectral properties and is concentration independent, only changing with temperature, pH, and molecular interactions.<sup>29</sup>

Combined with multiphoton tomography, MPT-FLIM is a powerful means of analyzing fluorophore populations and interactions in tissues. Traditional confocal microscopy is a linear optical process that uses a single-photon to excite a fluorophore and measure the subsequent fluorescent emission. The benefits of this method are low cost, compared to MPT systems, and widespread use. Single-photon confocal microscopy suffers from some drawbacks including scattering, photobleaching, limited depth penetration, and photodamage.<sup>30</sup> Multiphoton tomography, a much more expensive imaging technology, significantly reduces the effect of photobleaching and photodamage while increasing the depth at which tissues can be imaged.<sup>30,31</sup> While cost and complexity of running MPT systems has hindered widespread use, there are significant technological advantages. The MPT-FLIM system can measure fluorescence intensity, separate components of the skin, and quantify the fluorescence lifetime of NAD(P)H without significant variation within or between samples (Fig. 1). Figure 1 also includes photon-normalized spectra redrawn from previous work.<sup>32,33</sup>

The fluorescence lifetimes for free and protein-bound NAD(P)H differ and are approximately 400 and 2000 ps, respectively,<sup>26,29,34,35</sup> with the ratio of free to protein-bound NAD(P)H being used as an indicator of the cellular NADH/NAD<sup>+</sup> ratio state.<sup>36</sup> These data have been used to characterize NADH in breast cancer *in vitro* cell lines<sup>36</sup> as well as to differentiate between normal, precancerous, and cancerous epithelia of various grades<sup>37–40</sup> and to define meta-

bolic changes during apoptosis and necrosis.<sup>21</sup>

Both NADH and NADPH share the same absorption and fluorescence spectra,<sup>41</sup> though neither NAD<sup>+</sup> nor NADP<sup>+</sup> are fluorescent.<sup>41,42</sup> Additionally, these molecules possess the same fluorescence lifetime and are often used for live metabolic and free:bound NAD(P)H ratio imaging.<sup>26,41</sup> NADH is a central coenzyme molecule in several energy metabolic pathways, including anaerobic glycolysis, the electron transport chain, and the citric acid cycle.<sup>43</sup> Intracellular NADH concentration and distribution are useful and natural metabolic indicators because they are sensitive to pathological and physiological changes.<sup>36,40,44</sup> NADPH is a reducing agent that can counter the accumulation of reactive oxygen species<sup>20</sup> (ROS).

Studies have concluded that the relative fractions of free and protein-bound NAD(P)H, which can be inferred from the measured fluorescence lifetime,<sup>36</sup> can influence the cell redox state, defined by the ratio<sup>36,41</sup>  $[\text{NAD(P)H}]/[\text{NAD(P)}^+]$ . Different rates of electron transfer are likely to prevail in the free and bound states.

In this study, we used the autofluorescence and fluorescence lifetime properties of NAD(P)H to monitor the metabolic deterioration of *ex vivo* skin stored at different temperatures in the presence and absence of nutrient media over a 7-day time course. Two controls were used: images of the *ex vivo* skin taken at day 0 and *in vivo* images of the ventral forearm from three volunteers. We showed that MPT-FLIM of *ex vivo* skin yields characteristic and reproducible imaging data that can be used to monitor ischemic necrosis. These observations may contribute to the development of an optical assay for clinicians and researchers to assess the viability of skin flaps, preserved skin for transplants as well as *ex vivo* skin for experimentation that is metabolically comparable to *in vivo* skin.

## 2 Results

### 2.1 Autofluorescence Live Images

Figure 2 shows representative autofluorescence images of *in vivo* and *ex vivo* skin, at day 0, and *ex vivo* skin stored in the presence and absence of media at the indicated temperatures over the 7-day time course. *Ex vivo* skin stored at 4 °C in the absence of media maintained the most consistent autofluorescence with time (Fig. 2). Skin stored at 4 °C in media and at either –20 °C or room temperature without media showed less consistency. Autofluorescence was lost rapidly under the other conditions studied.

### 2.2 Autofluorescence Intensity and Photon Counts of NAD(P)H, Keratin, and FAD

Fluorescence intensity and NAD(P)H photon counts (total and normalized to either FAD or keratin photon counts) for each of the samples are shown in Fig. 3. Autofluorescence intensity and NAD(P)H photon counts (total and normalized) were relatively constant over time at 4 °C and at room temperature except at day 7. In contrast, tissue incubated at 37 °C exhibited a significant decrease ( $p < 0.05$ ) in autofluorescence intensity at day 1, which progressively decreased to zero over time (Fig. 3). A similar pattern was seen for the FAD-normalized NAD(P)H photon count with temperature and over time.

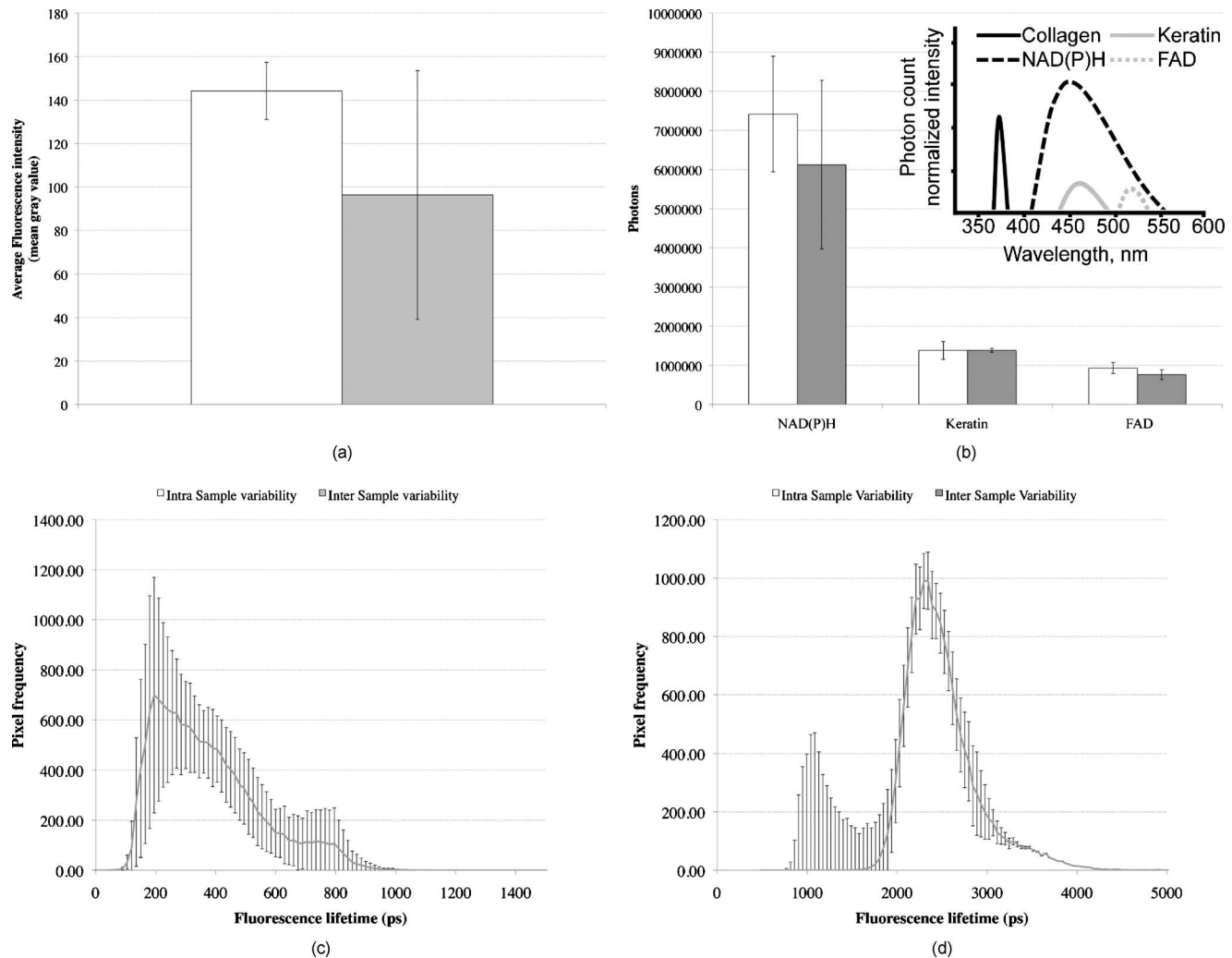


**Fig. 1** Fluorescence intensity and NAD(P)H lifetime intra and inter sample variation ( $n=6$ ) in study subjects. The images were acquired with a scan speed of  $512 \times 512$  pixels/13.6 s at  $52 \times 52 \mu\text{m}$  in size. (a) The average fluorescence intensity and standard deviation (SD) were calculated for the six subjects. (b) The photon contribution variability of NAD(P)H, keratin and FAD; the inset illustrates the photon normalized spectra redrawn from Zvyagin et al.<sup>33</sup> (c) and (d) The mean and SD of the average fast ( $\tau_1$ ) and slow ( $\tau_2$ ) NAD(P)H fluorescence lifetime decays, respectively.

### 2.3 Fluorescence Lifetime Distribution Histograms

Figure 4 shows the histograms of the lifetimes of the fast [ $\tau_1$ , free NAD(P)H] and slow decay components [ $\tau_2$ , protein-bound NAD(P)H] for both the *in vivo* and *ex vivo* controls. There was a major peak at  $\sim 400$  ps for both *in vivo* and *ex vivo* lifetime histograms for free NAD(P)H. A secondary peak at  $\sim 800$  ps was seen in *ex vivo* but not *in vivo* skin. A peak was also seen at  $\sim 2500$  ps with an additional peak at  $\sim 4500$  ps. In general, *ex vivo* skin samples kept at  $4^\circ\text{C}$  for 7 days without media showed two histogram peaks at  $\sim 500$  ps and  $\sim 2500$  to  $3500$  ps, comparable to the *in vivo* and *ex vivo* controls. Other samples showed much less consistency and other multiple peaks.

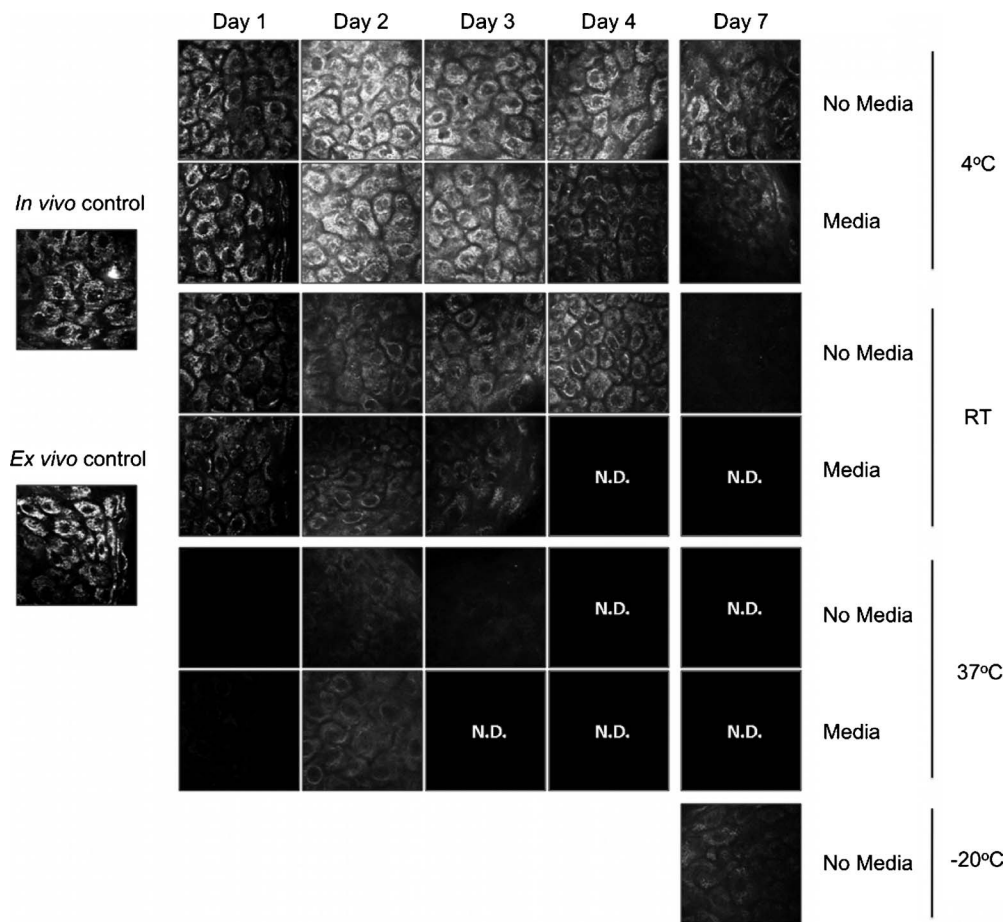
### 2.4 Free:Bound NAD(P)H Lifetime Ratio Images

Figure 5 shows representative pseudocolored images, between the  $\tau_m$  range of 0 to 2000 ps, of *in vivo* control and *ex vivo* skin samples stored over 7 days. The *in vivo* and *ex vivo* controls had a mean  $\tau_m$  fluorescence lifetime of  $\sim 1000$  ps. *Ex*

*in vivo* skin stored at  $4^\circ\text{C}$ , without media, maintained this mean lifetime up to 7 days. With media, mean lifetime of skin kept at  $4^\circ\text{C}$  was comparable to the controls only up to 4 days. For the remaining conditions, the mean lifetime progressively approached  $\sim 2000$  ps until tissue expiration.

### 2.5 Image Quality

Figure 6 displays the average image quality measurement (IQM) values over time of the imaged skin for each storage condition. Image quality for all the storage conditions initially increased after 24 h relative to the day 0 control. For skin stored at  $4^\circ\text{C}$ , with and without media, this value fell to the control level and persisted up until day 7. Figure 6 also shows that mean peak signal-to-noise ratio (PSNR) values from the *ex vivo* skin images stored at different conditions did not significantly change with time. However, the mean PSNR was higher for skin stored at  $37^\circ\text{C}$ , without media than at  $4^\circ\text{C}$  and room temperature without media, after 4 days. The noise frequency spectrum profiles are displayed in Fig. 7. Figure 7



**Fig. 2** Autofluorescence of *ex vivo* skin kept at 4 °C, room temperature (RT), and 37 °C in the presence and absence of nutrient media. The scale bar represents a distance of 10  $\mu\text{m}$ . The skin depths of the images range between 30 and 50  $\mu\text{m}$ . The absence of native cellular autofluorescence is indicated by N.D. (no detection).

aligns the autofluorescence images adjacent to their respective noise frequency spectra. Autofluorescence images representing viable epidermal cells (i.e., the controls and *ex vivo* skin at 4 °C) all displayed an L-shaped noise frequency spectrum. In contrast, tissues with high background/noise typical of cells damaged due to ischemic necrosis, such as *ex vivo* skin kept at 37 °C and -20 °C, showed a flat noise frequency spectrum.

### 3 Discussion

Previous studies demonstrate that cell death can alter NAD(P)H autofluorescence intensity in human cells. For example, autofluorescence increases during the early stages of apoptosis in primary human epithelial cells treated with cisplatin.<sup>22</sup> Ischemia has been well described to cause a physical reduction in NAD(P)H and a corresponding decrease in autofluorescence in a variety of cells and tissues.<sup>23,45,46</sup> The correlation with NADH autofluorescence intensity is related<sup>47</sup> to the physical concentration of the NADH. NADH autofluorescence has been used to assess the onset of skin flap necrosis in rats and showed a significant decrease in autofluorescence with time and necrosis.<sup>48</sup> In this study, a progressive loss of tissue autofluorescence intensity and FAD-normalized NAD(P)H photon counts occurred for *ex vivo* skin kept at 37 °C and to a lesser extent at room temperature. *Ex vivo* skin

kept at 4 °C maintained autofluorescence across the 7-day time course, which agrees with previous findings<sup>4,11,18,49</sup> based on the MTT assay that the metabolic viability of *ex vivo* skin was prolonged at 4 °C.

Our results also appear to parallel the decrease in NAD(P)H autofluorescence in yeast cells after reversible injury by the addition of  $\text{H}_2\text{O}_2$  or  $\text{ONOO}^-$  to stimulate oxidative stress.<sup>23</sup> As the epidermal cells in our experiment were progressing through ischemic necrosis, the reduction in autofluorescence may represent an initial depletion of NAD(P)H while the cells respond to metabolic demands and antioxidant responses, which are also associated with cell death.<sup>23,50,51</sup> In the *ex vivo* skin we examined, the recovery of autofluorescence and thus NAD(P)H levels may be due to a temporary burst of metabolic activity stimulated by ischemic-injury-induced damage and response systems.

In contrast, hepatocytes undergo an initial increase in autofluorescence from NADH during the early stages of hypoxia following reversible hypoxic injury.<sup>46</sup> When hepatocytes were exposed to longer hypoxic conditions, the autofluorescence gradually decreased from a peak level below the control until irreversible damage and cell death due to ischemia had occurred.<sup>46</sup> These changes occurred within 60 to 90 min after hypoxia. A similar trend was seen in this study, with the au-

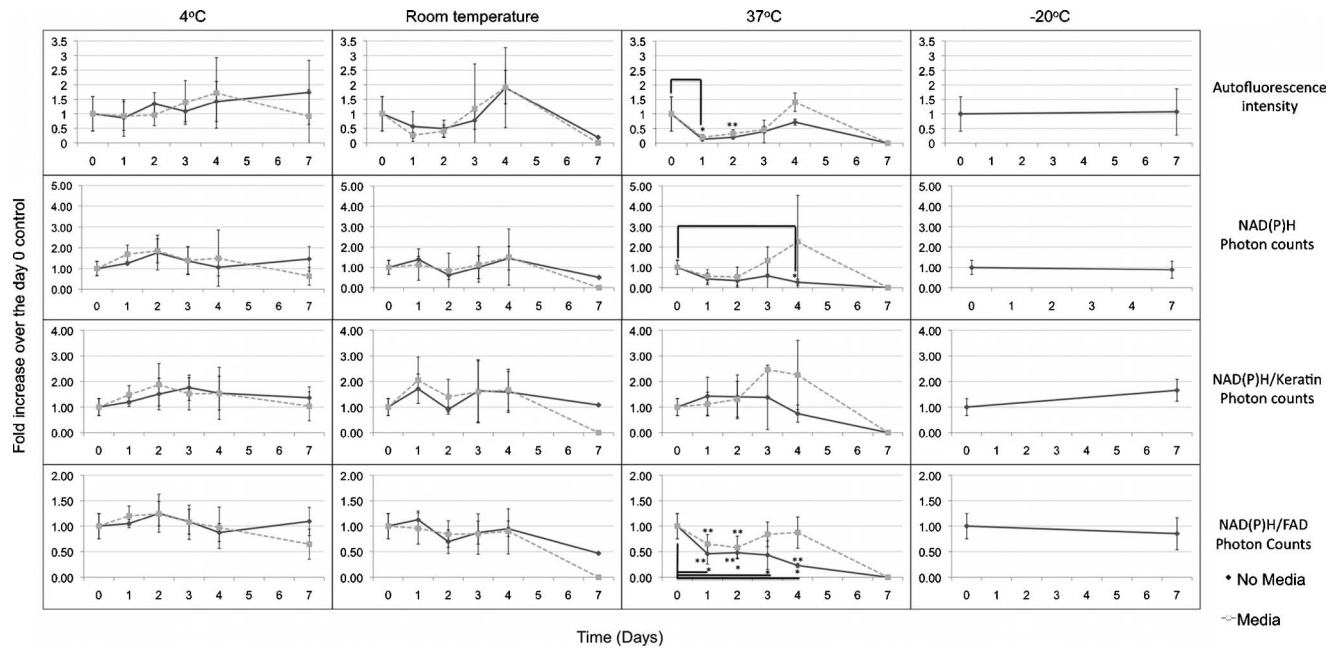


**Fig. 3** Autofluorescence intensity and photon counts of NAD(P)H, keratin and FAD from *ex vivo* skin stored at 4 °C, room temperature, and 37 °C. The mean fluorescence intensities of the autofluorescence images from 350 to 620 nm are shown in the first row. The second row plots the mean photon counts of NAD(P)H, as obtained from FLIM channel 1 (350 to 450 nm). The third row shows normalized NAD(P)H photon counts to keratin photon counts, determined from FLIM channel 2 (450 to 515 nm). The final row shows normalized NAD(P)H photon counts to FAD photon counts, calculated from FLIM channel 3 (515 to 620 nm). The error bars represent the SD of the means from three independent *ex vivo* skin samples.

tofluorescence of the *ex vivo* skin initially increasing after 24 to 48 h incubation at 4 °C and room temperature (Fig. 2). Speculatively, the increase in autofluorescence may be due to hypoxic injury or alterations in metabolic pathways. By the end of the 7-day time course, all autofluorescence had been lost for tissue kept at room temperature, indicating cell death. In skin, this peak occurred at 4 days in both the room temperature and 37 °C groups (Fig. 3). Although the trend in autofluorescence is similar in hepatocytes and skin, the time scale and temperature aspects do not clearly correlate. More investigation is required to fully understand the mechanisms that contribute to this phenomenon.

The absence of oxygen delivery to the viable epidermis in *ex vivo* skin may cause a significant dependence on anaerobic respiration for ATP production. The by-product of increased glycolysis is the production of lactate, which has been demonstrated to stimulate the production of reactive oxygen species.<sup>52</sup> Studies that have found lactate-stimulated ROS generation noted that this occurred while some mitochondrial respiration was active. A similar effect may be occurring in viable epidermis cells as the remaining oxygen levels within the skin, postexcision, would be depleted over time with further metabolic activity. Mitochondrial respiration would eventually be superseded by glycolysis in the viable epidermis as oxygen levels decrease and lactate production increases. This transition period may be a source of ROS generation and subsequent oxidative injury that takes place in the skin.

The loss of NAD(P)H autofluorescence was not seen in skin kept at 4 °C (Fig. 2). This may be due to the low temperature that significantly suppressed any metabolic activity,<sup>8</sup> irrespective of the presence of media. Generally, cellular au-

tofluorescence for skin kept at room temperature and 37 °C lasted longer in the absence of media (Fig. 2). This may be explained by the supply of metabolic nutrients in media to promote higher metabolic activity, and thus the accumulation of metabolic waste. If this were the case, the presence of media would accelerate the path toward ischemic necrosis. This hypothesis has been suggested in a similar study conducted by others.<sup>8</sup>

The mean lifetimes of free and protein-bound NAD(P)H (~400 and 2500 ps, respectively) closely matched other *in vitro* measurements.<sup>27,29</sup> Additionally, the values of the *in vivo* and *ex vivo* stratum spinosum fluorescence lifetimes ( $\tau_2$ ) agreed with another study.<sup>53</sup> Throughout the time course we observed the emergence of an additional  $\tau_1$  peak lifetime between 800 and 900 ps in addition to the control peak at ~400 ps in some skin samples (Fig. 4). The appearance of this peak was a common pattern for skin that had lost autofluorescence prior to tissue expiration. Similarly, for protein-bound NAD(P)H, a broad right-tailed histogram peak at ~2500 ps was also observed. The formation of these additional lifetime profiles may correlate with the interaction of NAD(P)H with an intracellular enzyme. This may be similar to the different lifetimes seen for NAD(P)H when bound to lactose dehydrogenase or mitochondrial malate dehydrogenase<sup>25</sup> (mMDH). Interestingly, the recorded  $\tau_1$  fluorescence lifetime of a solution of NADH:mMDH is<sup>25</sup> ~800 ps. Thus, the formation of the 800 ps  $\tau_1$  peak in Fig. 4(a) may be indicative of NADH binding to mMDH. There are also suggestions<sup>36,40,44</sup> that similar  $\tau_1$  peaks can be attributed to extended and folded populations of free NADH. How-

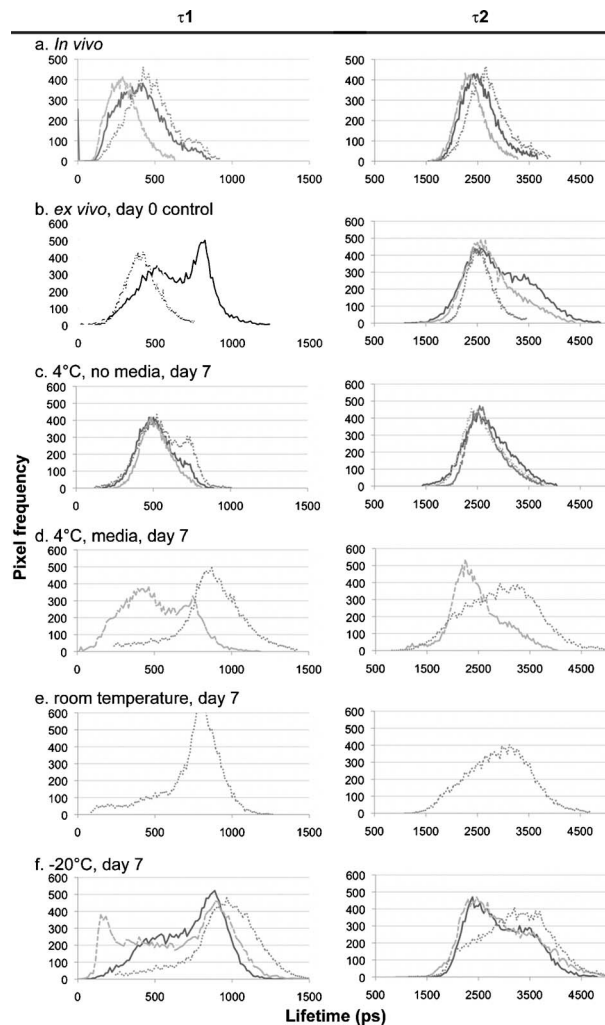


**Fig. 4** Free ( $\tau_1$ ) and protein-bound ( $\tau_2$ ) NAD(P)H fluorescence lifetime histograms of *in vivo* and *ex vivo* skin stored at 4 °C, room temperature, and -20 °C in the presence and absence of media. The fluorescence lifetime histograms of free and protein-bound NAD(P)H from FLIM imaged *ex vivo* skin are shown from day 7 of the time course. The separate histograms in each box represent *ex vivo* skin samples from up to three individuals.

ever, the relationships between these observations and the death of skin are not known. Similarly, the appearance of a  $\sim 3500$ -ps peak in the  $\tau_2$  histogram may be indicative of NADPH binding to NADPH oxidase (Nox2), which displays a comparable lifetime for this interaction.<sup>54</sup> Interestingly, Nox2 is involved in the production of ROS in endothelial cells in response to various agonists and stimulants.<sup>55</sup> One study also found that Nox2  $-/-$  mice displayed impaired neovascularization in response to ischemia, as Nox2 is involved in angiogenesis within endothelial cells via ROS production.<sup>55</sup> Further studies are necessary to determine whether these hypothetical interactions occur under these conditions.

The increase in the fluorescence lifetimes of NAD(P)H for skin undergoing ischemic necrosis contrasts with the decrease in lifetime recorded for *in vitro* cells treated with potassium cyanide (KCN), a metabolic inhibitor.<sup>36</sup> The authors concluded<sup>36</sup> that the decrease of fluorescence lifetime corre-

lated with an increase in the NADH/NAD<sup>+</sup> ratio, potentially due to the underutilization of NADH resulting from the inhibition of the electron transport chain by KCN. In this study however, the *ex vivo* skin suffering from ischemic necrosis does not have a fresh source of nutrients and a means of extracting waste. Thus, the lack of nutrients during continued metabolic activity may inhibit the replenishing of fresh NADH/NADPH and lead to the accumulation of NAD<sup>+</sup>/NADP<sup>+</sup>.

FLIM images of cultured cells pseudocolored by the mean fluorescence lifetime and weighted by relative amplitudes of components ( $\tau_m$ ) have been used as a visual indicator of the cellular free:bound NAD(P)H ratio state and related to cancer progression.<sup>36,38</sup> In our study, the progressive increase of the mean  $\tau_m$  lifetime from  $\sim 1000$  to  $\sim 2000$  ps appears to be an indicator of ischemic necrosis. Interestingly, these results contrast with other studies that have described the average  $\tau_m$  lifetime decreasing with hypoxia in cancerous tissue.<sup>38,39</sup> While a marked decrease in the supply of oxygen during metabolic activity is common to these physiological states, the contrast in fluorescence lifetimes may be explained by the finding that human epidermal skin metabolism is already predominantly anaerobic.<sup>56</sup> Thus, the lifetime increases throughout the onset of ischemic necrosis may be more related to removal of metabolic waste from the tissue via the vasculature rather than the lack of oxygen supply. Further studies are required to examine this hypothesis.

Noise frequency spectra have been largely used to assess noise compensation or filter software for digital cameras, with flat spectra indicating uncompensated white noise.<sup>57</sup> Cameras that use digital software to compensate for white noise display a roll-off in noise frequency spectra, characteristic of spectral noise.<sup>57</sup> We found that tissue with advanced ischemic necrosis gave a cloudy image, presumably due to leaking intracellular material.<sup>58</sup> In addition, there was a flat noise frequency spectrum rather than the L-shaped spectrum seen for the control images and the best-preserved tissue stored at 4 °C up to 7 days (Fig. 7).

In summary, this study has examined changes in NAD(P)H autofluorescence following the progressive onset of ischemic necrosis in *ex vivo* skin. We have found that ischemic necrosis of the tissue is marked by several characteristics: (1) a loss in NAD(P)H autofluorescence, possibly due to a physical depletion of the molecule; (2) a reduction in the FAD normalized NAD(P)H photon count; (3) a significant deviation in the fluorescence lifetime histogram of free and protein-bound NAD(P)H away from a normal "control" state (i.e., freshly excised *ex vivo* skin); (4) an increase in the  $\tau_m$  average fluorescence lifetime above  $\sim 1000$  ps; and (5) a qualitative loss is cellular integrity, revealed by noise frequency spectra analysis. These patterns may serve as the basis for MPT-FLIM to be used as a visual noninvasive biopsy for assessing the onset of ischemic necrosis of *ex vivo* skin.

## 4 Materials and Methods

### 4.1 DermalInspect/MPT-FLIM

Multiphoton tomography was carried out using the DermalInspect system (JenLab GmbH, Jena, Germany). Excitation light for multiphoton imaging was provided by an ultra-short-

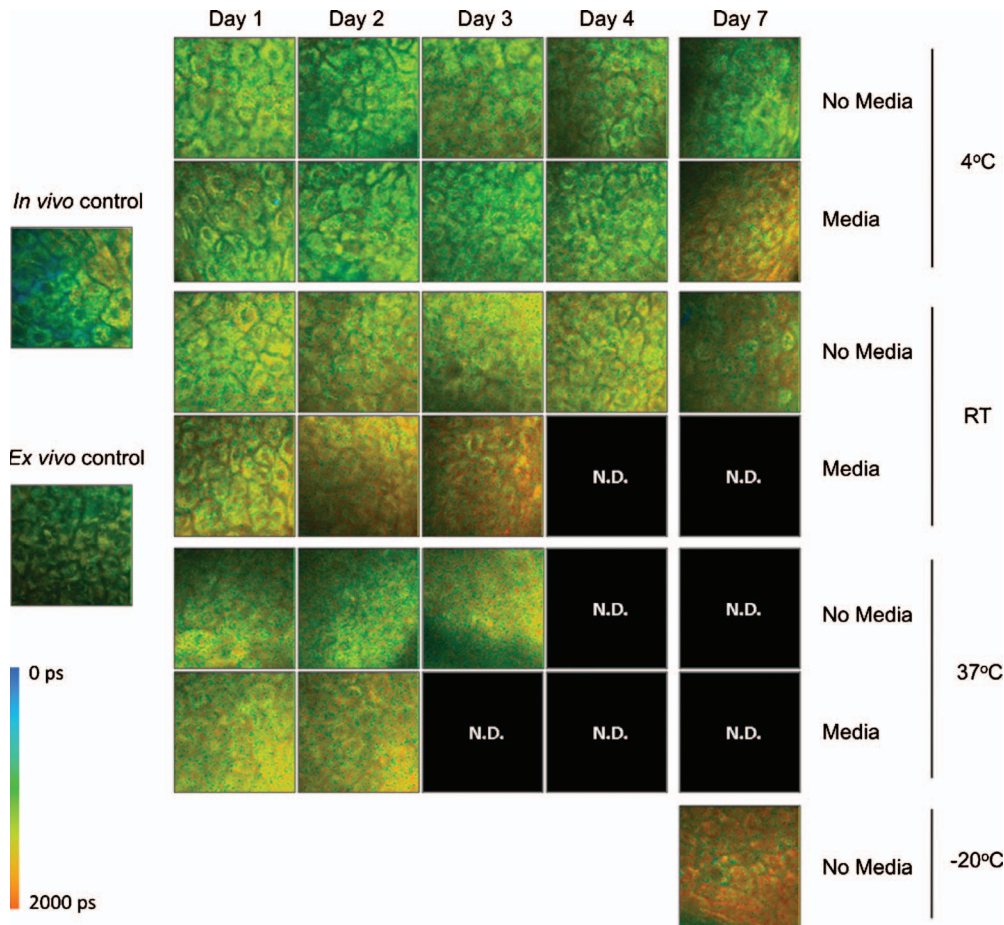


**Fig. 5** Fluorescence lifetime images of *ex vivo* skin kept in the presence and absence of media, at various temperatures, across a 7-day time course. The images have been pseudocolored according to  $\tau_m$ , which is calculated by weighting the mean fluorescence lifetime of free and protein-bound NAD(P)H ( $\tau_1$  and  $\tau_2$ , respectively) by their respective contributions:  $\alpha_1$  and  $\alpha_2$ . These are representative images taken from three independent experiments.

pulsed (85-fs pulse width) mode-locked 80-MHz titanium sapphire laser (MaiTai, Spectraphysics, Mountain View, California). The tuning range of the excitation wavelength was 710 to 920 nm. To enable FLIM measurements, a time-correlated single-photon counting SPC 830 FLIM system (Becker & Hickl, Berlin, Germany) was integrated into the

tomography system. FLIM analyses were performed by an SPC 830 2.9 software module installed on a dual core computer with a Windows XP operating system. The SPC module builds<sup>59</sup> a photon distribution over the  $x$  and  $y$  scan coordinates along with the time within the fluorescence decay,  $\tau$ .

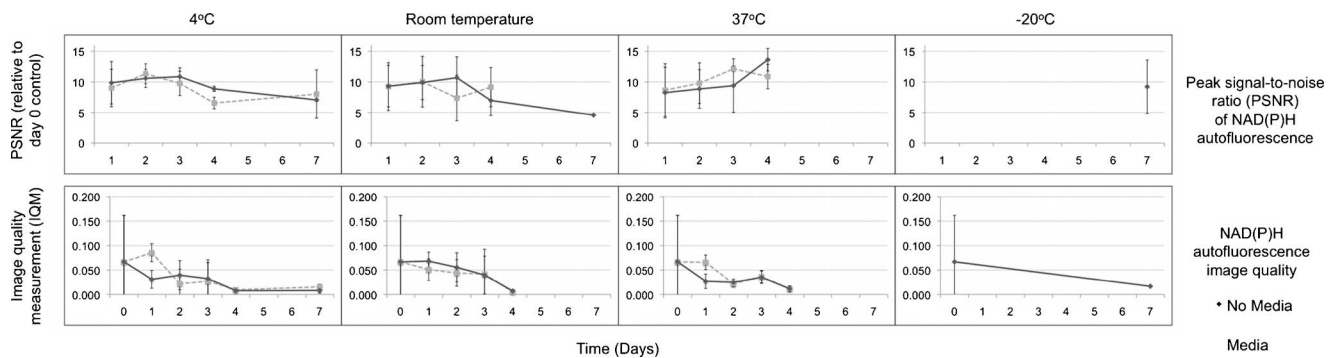


**Fig. 6** Mean PSNRs of the autofluorescence images ( $\pm$ SD), relative to the day 0 control (upper) and “image quality” mean from *ex vivo* skin samples ( $\pm$ SD), from the three study subjects, across the 7-day time course (lower). PSNRs were determined by ImageJ using a custom script. Autofluorescence images (Fig. 2) were processed with the image processing software Image Quality from a Natural Scene (MITRE, Bedford, Massachusetts) to obtain a quantitative IQM value.

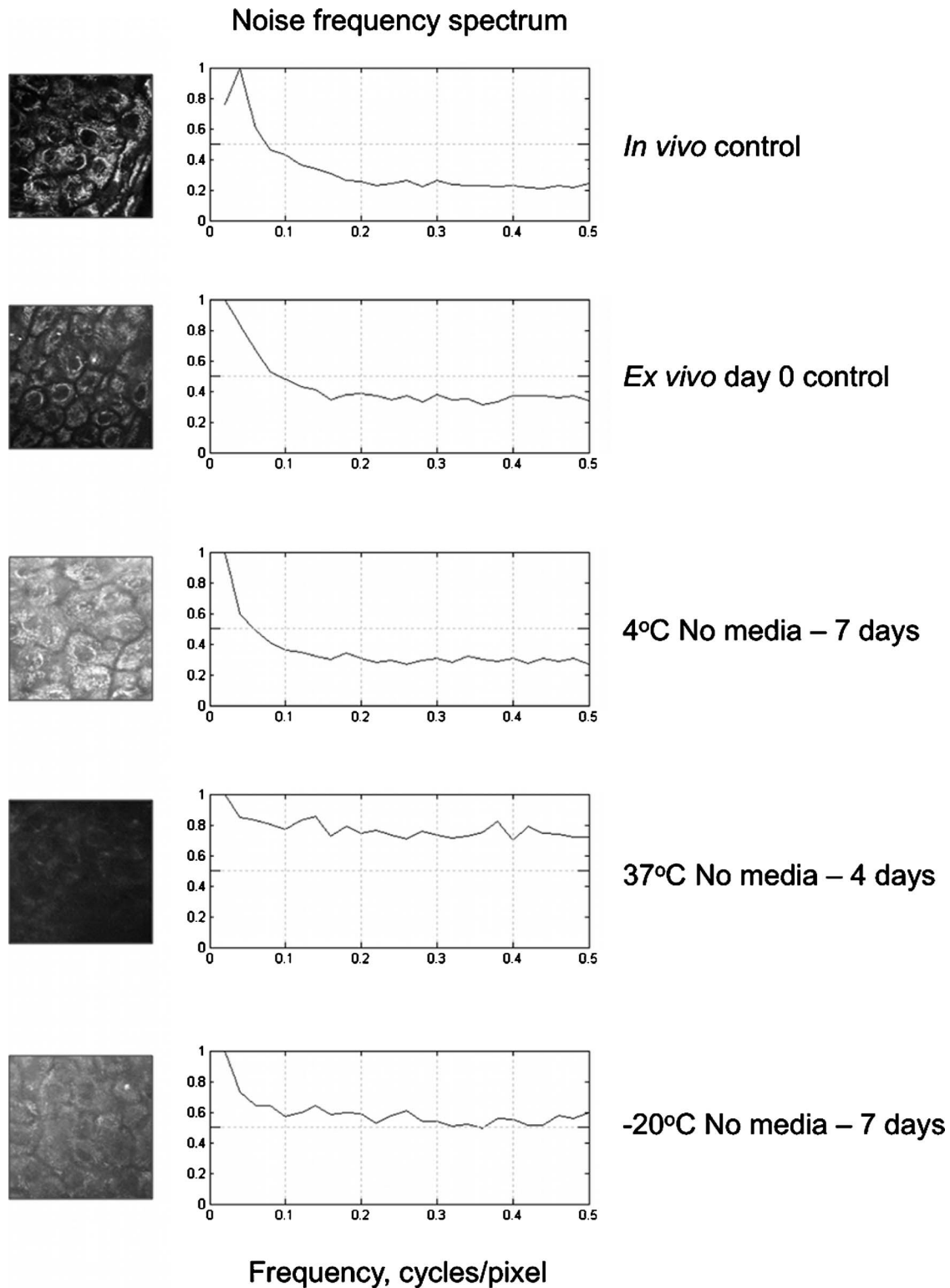


**Fig. 7** Noise frequency spectra of *in vivo* skin and *ex vivo* skin at day 0, 4 days at 37 °C (no media), and 7 days at 4 °C (no media), shown next to the corresponding representative autofluorescence image. The spectra were obtained by calculating the Fourier transform of the autofluorescence images using the software package Imatest (Imatest LCC, Boulder, Colorado). Data were collected from three independent experiments.

The signals from four photon-counting detectors operated at different wavelength intervals and were processed simultaneously.

To analyze the FLIM data, the software data analysis package SPCImage (Becker & Hickl GmbH, Berlin, Germany) was used. This package uses iterative convolution with either

a single-, double-, or triple-exponential model to calculate the decay parameters for each individual pixel within the scan. The amplitude weighted average  $\tau_m$  of the double-exponential fit was used to analyze the photon decay profiles from the scanned images of the epidermis unless otherwise noted. The resulting two components are  $\tau_1$  and  $\tau_2$ . When a tissue sample was excited with 740 nm (two-photon), the  $\tau_1$  and  $\tau_2$  fluorescence lifetime decay histograms have been shown to correlate with free and protein-bound NAD(P)H respectively within the cells.<sup>60</sup> Deviations away from these native fluorescence lifetimes indicate changes in the state of NAD(P)H within the cell. Changes in the fluorescence lifetime of NAD(P)H can be caused by alterations in temperature, pH and protein binding.<sup>61</sup>

The objective lens used in this study was the Plan-Neofluar oil-immersion 40 $\times$ /1.30 (Carl Zeiss, Germany) with the distance between the objective lens and the *in vivo* adaptor filled with index-matching oil. The MPT imaging system (JenLab GmbH, Jena, Germany) uses ultra-short-pulse excitation laser light that is narrowly focused onto a sample via a high-numerical-aperture (NA) oil-immersion microscope objective (40 $\times$ , NA, 1.3). Two IR photons emitted by the ultrashort-pulsed-laser were simultaneously absorbed by a single fluorophore molecule, raising it to an excited state in a process known as two-photon excited fluorescence (TPEF). Through the objective, the focused laser light within the femtoliter focal volume in the sample resulted in a large and instantaneous intensity that caused the sample's nonlinear optical response. The fluorescence emission occurred exclusively within the focal volume. This resulted essentially in an "optical section," with the thickness of each section calculated by the axial transfer function of the imaging system, or 2  $\mu$ m with our instrument.

To image *ex vivo* and *in vivo* skin, the excitation wavelength was set to 740 nm (two-photon) with a laser power of 25mW at the sample to excite NAD(P)H, which is responsible for cellular autofluorescence. The focal point within the sample was raster-scanned using two galvanometer mirrors. The same objective lens was used to collect all emitted fluorescence, which was transmitted through a dichroic mirror and optical filter for detection by photon-multiplier tubes (PMTs). The dichroic mirror simultaneously reflects any IR laser excitation photons to prevent feedback. A BG39 filter (350 to 650 nm, Schott glass color filter) was used to optically filter the fluorescence light to either the live image or FLIM PMT. In front of the FLIM detectors, a 350 to 450-nm bandpass filter was used to isolate the NAD(P)H signal and the FAD signal was isolated with a 515 to 620-nm bandpass filter. All live and FLIM images were acquired with a scan speed of 512 $\times$ 512 pixels/13.6 s at a 52 $\times$ 52- $\mu$ m size. The skin was imaged at a depth range between 30 and 50  $\mu$ m, which encompassed the stratum spinosum. This range was necessary due to the undulating profile of the viable epidermis and subsequent variable depth of the stratum spinosum. The imaging depth was determined by keratinocyte morphology, with an emphasis on maintaining uniform cell diameter between samples.

#### 4.2 Skin Samples

Excised human abdomen skin samples from three individuals were obtained from volunteers immediately following elective

surgery. The donors gave informed written consent, and approval for the collection of the skin samples was given by the Princess Alexandra Hospital Research Committee (Approval no. 097/090, administered by the University of Queensland Human Ethics Committee). The skin samples were processed on delivery to remove the underlying fat and connective tissue. The resulting full-thickness skin was then cut into 2-cm-diam circles and placed into yellow-capped sample containers, either in the presence or absence of 1.5 ml of nutrient serum-free Dulbecco modified Eagle medium (DMEM). The media was not supplemented with antibiotics due to their metabolic effects on the *ex vivo* skin, as determined by FLIM (data not shown). For *in vivo* control images, a drop of water was placed on the ventral forearm of three individual volunteers, followed by a 170- $\mu$ m-thick microscope glass coverslip. Immersion oil was placed between the coverslip and the objective lens prior to imaging. Scan settings and depths were identical to those used for *ex vivo* skin samples.

#### 4.3 Time Course Incubations

The skin samples were stored at 4 °C, room temperature, or 37 °C, with a partially unscrewed lid to permit gas exchange, in the presence or absence of nutrient media. Samples kept at 37 °C were placed within a tissue culture incubator with 5% CO<sub>2</sub>. Skin was also stored at -20 °C without media for the incubation period. The control for this experiment was a sample of the skin imaged by MPT-FLIM prior to incubation at room temperature. Tissue stored at 4 °C, room temperature, and 37 °C was imaged every 24 h by MPT-FLIM over 96 h. After 7 days from the day of incubation (i.e., the day 0 control), the skin stored at -20 °C was thawed and imaged along with the remaining tissue samples.

#### 4.4 Autofluorescence Intensity and Photon Counts

The autofluorescence images were analyzed for fluorescence intensity using the Java-based image-processing program ImageJ (National Institutes of Health). The autofluorescence intensity from the images taken from three independent *ex vivo* skin samples, stored under the conditions already indicated, were averaged and plotted against the time course in days. Photon counts were obtained using the SPCImage software. FLIM data were separated by optical filters into three emission channels: channel 1 (350 to 450 nm), channel 2 (450 to 515 nm), and channel 3 (515 to 620 nm). An excitation wavelength of 740 nm (two-photon) was used to observe autofluorescence. A 350- to 450-nm bandpass filter was used to isolate NAD(P)H. Keratin and FAD were imaged through 450 to 515- and 515- to 620-nm bandpass filters, respectively. Using SPCImage, these channels were used to obtain and normalize NAD(P)H photon counts to keratin and FAD as a quantitative approach to measure the levels of this metabolic molecule within the image field of view.

#### 4.5 Free:Bound NAD(P)H Ratio Imaging

Both *in vivo* and the stored *ex vivo* skin imaged by FLIM was pseudocolored to display the mean lifetime weighted by their relative contributions of free and protein-bound NAD(P)H ( $\tau_m = \tau_1 \alpha_1 + \tau_2 \alpha_2$ ). This provided a qualitative representation of the free:bound NAD(P)H ratio of the tissue while provid-

ing an effective means of comparison to the control across the time course.

#### 4.6 Image Quality Analysis

To obtain a quantitative value for the level of image quality, in relation to noise distortion, we used the image processing software Image Quality from a Natural Scene (IQM; MITRE, Bedford, Massachusetts). Autofluorescence images (represented in Fig. 2) were processed to obtain an IQM value using an objective image quality system, which has been described.<sup>62</sup> The autofluorescence images were analyzed by IQM to obtain an arbitrary value for image quality, based on the level of noise and spatial image power spectrum. The second approach used to ascertain image quality was to measure the noise frequency spectra of the autofluorescence images using the software package Imatest (Imatest LCC, Boulder, Colorado). The noise frequency spectrum was obtained by calculating the Fourier transform of the spatial image.<sup>57</sup> Noise frequency spectrum analysis has been used to discern between white noise and spectral (nonwhite) noise.<sup>63</sup> White noise demonstrates a flat noise frequency spectrum profile while spectral noise possesses an L-shaped curve.<sup>63</sup> In this study, we attempted to use noise frequency spectrum analysis to differentiate between images where cellular integrity was high (i.e., *in vivo* and *ex vivo* day 0 controls) and low, due to ischemic necrosis (i.e., cell images prior to tissue expiration). The final approach used the program ImageJ again to measure the PSNR, using a custom script. The *ex vivo* day 0 control served as the reference image for autofluorescence images across the time course, for each respective individual.

#### 4.7 Statistical Analysis

Results were expressed as mean  $\pm$  standard deviation (SD). Statistical significance was ascertained by using a Student's *t* test, with a *p* value less than 0.05 considered statistically significant.

#### Acknowledgments

We acknowledge the support of the Australian National Health & Medical Research Council (NHMRC) and the Asian Office of Research and Development (AORD) in undertaking this work. The authors state no conflict of interest.

#### References

- G. K. Menon, "New insights into skin structure: scratching the surface," *Adv. Drug Delivery Rev.* **54**(Suppl. 1), S3–17 (2002).
- B. Godin and E. Touitou, "Transdermal skin delivery: predictions for humans from *in vivo*, *ex vivo* and animal models," *Adv. Drug Delivery Rev.* **59**(11), 1152–1161 (2007).
- R. C. Wester, and H. I. Maibach, "Percutaneous absorption of drugs," *Clin. Pharm.* **23**(4), 253–266 (1992).
- H. Ben-Bassat, "Performance and safety of skin allografts," *Clin. Dermatol.* **23**(4), 365–375 (2005).
- M. H. Hermans, "Clinical experience with glycerol-preserved donor skin treatment in partial thickness burns," *Burns Incl Therm Inj.* **15**(1), 57–59 (1989).
- E. S. Kalter and T. M. de By, "Tissue banking programmes in Europe," *Br. Med. Bull.* **53**(4), 798–816 (1997).
- D. Alotto, S. Ariotti, S. Graziano, R. Verrua, M. Stella, G. Magliacani, and C. Castagnoli, "The role of quality control in a skin bank: tissue viability determination," *Cell Tissue Bank* **3**(1), 3–10 (2002).
- J. N. Kearney, "Guidelines on processing and clinical use of skin allografts," *Clin. Dermatol.* **23**(4), 357–364 (2005).
- A. R. Compañen, L. I. van der Wel, L. Wei, J. D. Laman, and E. P. Prens, "A modified *ex vivo* skin organ culture system for functional studies," *Arch. Dermatol. Res.* **293**(4), 184–90 (2001).
- C. Gelis, A. Mavon, M. Delverdier, N. Paillous, and P. Vicendo, "Modifications of *in vitro* skin penetration under solar irradiation: evaluation on flow-through diffusion cells," *Photochem. Photobiol.* **75**(6), 598–604 (2002).
- D. Bravo, T. H. Rigley, N. Gibran, D. M. Strong, and H. Newman-Gage, "Effect of storage and preservation methods on viability in transplantable human skin allografts," *Burns* **26**(4), 367–378 (2000).
- C. Antille, C. Tran, O. Sorg, and J. H. Saurat, "Penetration and metabolism of topical retinoids in *ex vivo* organ-cultured full-thickness human skin explants," *Skin Pharmacol. Physiol.* **17**(3), 124–128 (2004).
- N. A. Monteiro-Riviere, A. O. Inman, T. H. Snider, J. A. Blank, and D. W. Hobson, "Comparison of an *in vitro* skin model to normal human skin for dermatological research," *Microsc. Res. Tech.* **37**(3), 172–179 (1997).
- N. Issachar, Y. Gall, M. T. Borell, and M. C. Poelman, "pH measurements during lactic acid stinging test in normal and sensitive skin," *Contact Dermatitis* **36**(3), 152–155 (1997).
- S. Messenger, A. C. Hann, P. A. Goddard, P. W. Dettmar, and J. Y. Maillard, "Assessment of skin viability: is it necessary to use different methodologies?" *Skin Res. Technol.* **9**(4), 321–330 (2003).
- M. A. Zieger, E. E. Tredget, and L. E. McGann, "A simple, effective system for assessing viability in split-thickness skin with the use of oxygen consumption," *J. Burn Care Rehabil.* **14**(3), 310–318 (1993).
- H. L. Bank and M. K. Schmehl, "Parameters for evaluation of viability assays: accuracy, precision, specificity, sensitivity, and standardization," *Cryobiology* **26**(3), 203–211 (1989).
- C. Castagnoli, D. Alotto, I. Cambieri, R. Casimiri, M. Aluffi, M. Stella, S. T. Alasia, and G. Magliacani, "Evaluation of donor skin viability: fresh and cryopreserved skin using tetrazolium salt assay," *Burns* **29**(8), 759–767 (2003).
- M. B. Klein, D. Shaw, S. Barese, G. A. Chapo, and C. B. Cuono, "A reliable and cost-effective *in vitro* assay of skin viability for skin banks and burn centers," *J. Burn Care Rehabil.* **17**(6 Pt 1), 565–570 (1996).
- W. Ying, "NAD<sup>+</sup>/NADH and NADP<sup>+</sup>/NADPH in cellular functions and cell death: regulation and biological consequences," *Antioxid. Redox. Signal.* **10**(2), 179–206 (2008).
- H. W. Wang, V. Gukassyan, C. T. Chen, Y. H. Wei, H. W. Guo, J. S. Yu, and F. J. Kao, "Differentiation of apoptosis from necrosis by dynamic changes of reduced nicotinamide adenine dinucleotide fluorescence lifetime in live cells," *J. Biomed. Opt.* **13**(5), 054011 (2008).
- J. M. Levitt, A. Baldwin, A. Papadakis, S. Puri, J. Xylas, K. Munger, and I. Georgakoudi, "Intrinsic fluorescence and redox changes associated with apoptosis of primary human epithelial cells," *J. Biomed. Opt.* **11**(6), 064012 (2006).
- J. Liang, W. L. Wu, Z. H. Liu, Y. J. Mei, R. X. Cai, and P. Chen, "Study the oxidative injury of yeast cells by NADH autofluorescence," *Spectrochim. Acta A Mol. Biomol. Spectrosc.* **67**(2), 355–359 (2007).
- Q. Yu, M. Proia, and A. A. Heikal, "Integrated biophotonics approach for noninvasive and multiscale studies of biomolecular and cellular biophysics," *J. Biomed. Opt.* **13**(4), 041315 (2008).
- Q. Yu and A. A. Heikal, "Two-photon autofluorescence dynamics imaging reveals sensitivity of intracellular NADH concentration and conformation to cell physiology at the single-cell level," *J. Photochem. Photobiol., B* **95**(1), 46–57 (2009).
- H. Schneckenburger and K. König, "Fluorescence decay kinetics and imaging of NAD(P)H and flavins as metabolic indicators," *Opt. Eng.* **31**(7), 1447–1451 (1992).
- V. K. Ramanujan, J. H. Zhang, E. Biener, and B. Herman, "Multi-photon fluorescence lifetime contrast in deep tissue imaging: prospects in redox imaging and disease diagnosis," *J. Biomed. Opt.* **10**(5), 051407 (2005).
- P. I. Bastiaens and A. Squire, "Fluorescence lifetime imaging microscopy: spatial resolution of biochemical processes in the cell," *Trends Cell Biol.* **9**(2), 48–52 (1999).
- J. R. Lakowicz, H. Szmajdzinski, K. Nowaczyk, and M. L. Johnson, "Fluorescence lifetime imaging of free and protein-bound NADH," *Proc. Natl. Acad. Sci. U.S.A.* **89**(4), 1271–1275 (1992).
- R. M. Williams, D. W. Piston, and W. W. Webb, "Two-photon molecular excitation provides intrinsic 3-dimensional resolution for laser-based microscopy and microphotochemistry," *FASEB J.* **8**(11),

- 804–813 (1994).
31. J. Paoli, M. Smedh, and M. B. Ericson, "Multiphoton laser scanning microscopy—a novel diagnostic method for superficial skin cancers" *Semin Cutan Med. Surg.* **28**(3), 190–195 (2009).
  32. M. S. Roberts, M. J. Roberts, T. A. Robertson, W. Sanchez, C. Thorling, Y. Zou, X. Zhao, W. Becker, and A. V. Zvyagin, "In vitro and in vivo imaging of xenobiotic transport in human skin and in the rat liver" *J. Biophoton.* **1**(6), 478–493 (2008).
  33. A. V. Zvyagin, X. Zhao, A. Gierden, W. Sanchez, J. A. Ross, and M. S. Roberts, "Imaging of zinc oxide nanoparticle penetration in human skin *in vitro* and *in vivo*," *J. Biomed. Opt.* **13**(6), 064031 (2008).
  34. H. Schneckenburger, M. H. Gschwend, W. S. Strauss, R. Sailer, M. Kron, U. Steeb, and R. Steiner, "Energy transfer spectroscopy for measuring mitochondrial metabolism in living cells," *Photochem. Photobiol.* **66**(1), 34–41 (1997).
  35. K. Konig, "Clinical multiphoton tomography," *J. Biophoton.* **1**(1), 13–23 (2008).
  36. D. K. Bird, L. Yan, K. M. Vrotsos, K. W. Eliceiri, E. M. Vaughan, P. J. Keely, J. G. White, and N. Ramanujam, "Metabolic mapping of MCF10A human breast cells via multiphoton fluorescence lifetime imaging of the coenzyme NADH" *Cancer Res.* **65**(19), 8766–8773 (2005).
  37. M. W. Conklin, P. P. Provenzano, K. W. Eliceiri, R. Sullivan, and P. J. Keely, "Fluorescence lifetime imaging of endogenous fluorophores in histopathology sections reveals differences between normal and tumor epithelium in carcinoma *in situ* of the breast," *Cell Biochem. Biophys.* **53**(3), 145–157 (2009).
  38. M. C. Skala, K. M. Riching, A. Gendron-Fitzpatrick, J. Eickhoff, K. W. Eliceiri, J. G. White, and N. Ramanujam, "In vivo multiphoton microscopy of NADH and FAD redox states, fluorescence lifetimes, and cellular morphology in precancerous epithelia," *Proc. Natl. Acad. Sci. U.S.A.* **104**(49), 19494–19499 (2007).
  39. M. C. Skala, K. M. Riching, D. K. Bird, A. Gendron-Fitzpatrick, J. Eickhoff, K. W. Eliceiri, P. J. Keely, and N. Ramanujam, "In vivo multiphoton fluorescence lifetime imaging of protein-bound and free nicotinamide adenine dinucleotide in normal and precancerous epithelia," *J. Biomed. Opt.* **12**(2), 024014 (2007).
  40. I. Georgakoudi et al., "NAD(P)H and collagen as *in vivo* quantitative fluorescent biomarkers of epithelial precancerous changes," *Cancer Res.* **62**(3), 682–687 (2002).
  41. D. W. Piston, and S. M. Knobel, "Real-time analysis of glucose metabolism by microscopy," *Trends Endocrinol. Metab.* **10**(10), 413–417 (1999).
  42. B. Chance, V. Legallais, and B. Schoener, "Metabolically linked changes in fluorescence emission spectra of cortex of rat brain, kidney and adrenal gland," *Nature* **195**, 1073–1075 (1962).
  43. S. J. Lin and L. Guarente, "Nicotinamide adenine dinucleotide, a metabolic regulator of transcription, longevity and disease," *Curr. Opin. Cell Biol.* **15**(2), 241–246 (2003).
  44. H. D. Vishwasrao, A. A. Heikal, K. A. Kasischke, and W. W. Webb, "Conformational dependence of intracellular NADH on metabolic state revealed by associated fluorescence anisotropy," *J. Biol. Chem.* **280**(26), 25119–25126 (2005).
  45. J. T. Fitzgerald, S. Demos, A. Michalopoulou, J. L. Pierce, and C. Troppmann, "Assessment of renal ischemia by optical spectroscopy," *J. Surg. Res.* **122**(1), 21–28 (2004).
  46. E. T. Obi-Tabot, L. M. Hanrahan, R. Cachecho, E. R. Beer, S. R. Hopkins, J. C. Chan, J. M. Shapiro, and W. W. LaMorte, "Changes in hepatocyte NADH fluorescence during prolonged hypoxia," *J. Surg. Res.* **55**(6), 575–580 (1993).
  47. A. Mayevsky and G. G. Rogatsky, "Mitochondrial function *in vivo* evaluated by NADH fluorescence: from animal models to human studies," *Am. J. Physiol.: Cell Physiol.* **292**(2), C615–640 (2007).
  48. M. Mokry, P. Gal, M. Harakalova, Z. Hutnanova, J. Kusnir, S. Mozes, and J. Sabo, "Experimental study on predicting skin flap necrosis by fluorescence in the FAD and NADH bands during surgery," *Photochem. Photobiol.* **83**(5), 1193–1196 (2007).
  49. J. N. Kearney, "Quality issues in skin banking: a review," *Burns* **24**(4), 299–305 (1998).
  50. M. C. Gendron, N. Schrantz, D. Metivier, G. Kroemer, Z. Maciorowska, F. Sureau, S. Koester, and P. X. Petit, "Oxidation of pyridine nucleotides during Fas- and ceramide-induced apoptosis in Jurkat cells: correlation with changes in mitochondria, glutathione depletion, intracellular acidification and caspase 3 activation," *Biochem. J.* **353**(Pt. 2), 357–367 (2001).
  51. G. Kroemer, P. Petit, N. Zamzami, J. L. Vayssiere, and B. Mignotte, "The biochemistry of programmed cell death," *FASEB J.* **9**(13), 1277–1287 (1995).
  52. T. Hashimoto, R. Hussien, S. Oommen, K. Gohil, and G. A. Brooks, "Lactate sensitive transcription factor network in L6 cells: activation of MCT1 and mitochondrial biogenesis," *FASEB J.* **21**(10), 2602–2612 (2007).
  53. K. Konig, A. Ehlers, F. Stracke, and I. Riemann, "In vivo drug screening in human skin using femtosecond laser multiphoton tomography," *Skin Pharmacol. Physiol.* **19**(2), 78–88 (2006).
  54. R. Niesner, P. Narang, H. Spiecker, V. Andreson, K. H. Gericke, and M. Gunzer, "Selective detection of NADPH oxidase in polymorphonuclear cells by means of NAD(P)H-based fluorescence lifetime imaging," *J. Biophys.* **2008**, 602–639 (2008).
  55. M. Ushio-Fukai and Y. Nakamura, "Reactive oxygen species and angiogenesis: NADPH oxidase as target for cancer therapy," *Cancer Lett.* **266**(1), 37–52 (2008).
  56. G. Ronquist, A. Andersson, N. Bendsoe, and B. Falck, "Human epidermal energy metabolism is functionally anaerobic," *Exp. Dermatol.* **12**(5), 572–579 (2003).
  57. Imatest, "Imatest stepchart," *Digital Image Quality Testing 2009*; available from <http://www.imatest.com/guides/modules/stepchart>.
  58. G. Kroemer, B. Dallaporta, and M. Resche-Rigon, "The mitochondrial death/life regulator in apoptosis and necrosis," *Annu. Rev. Physiol.* **60**, 619–642 (1998).
  59. D. C. Dai, S. J. Xu, S. L. Shi, M. H. Xie, and C. M. Che, "Efficient multiphoton-absorption-induced luminescence in single-crystalline ZnO at room temperature," *Opt. Lett.* **30**(24), 3377–3379 (2005).
  60. T. G. Scott, R. D. Spencer, N. J. Leonard, and G. Weber, "Emission properties of NaDH. studies of fluorescence lifetimes and quantum efficiencies of NADH, AcPyADH, and simplified synthetic models," *J. Am. Chem. Soc.* **92**(3), 687–695 (1970).
  61. A. Gafni and L. Brand, "Fluorescence decay studies of reduced nicotinamide adenine dinucleotide in solution and bound to liver alcohol dehydrogenase," *Biochemistry* **15**(15), 3165–3171 (1976).
  62. N. B. Nill and B. H. Bouzas, "Objective image quality measure derived from digital image power spectra," *Opt. Eng.* **31**(4), 813–825 (1992).
  63. Imatest, "Noise in photographic images," *Digital Image Quality Testing 2009*; available from <http://www.imatest.com/docs/noise.html>.